# Curvature-dependent adsorption of water inside and outside armchair carbon nanotubes

Shulai Lei and Beate Paulus

*Institut für Chemie und Biochemie, Freie Universität Berlin,*

*Takustraße 3, D-14195 Berlin, Germany*

Shujuan Li and Burkhard Schmidt

*Institut für Mathematik, Freie Universität Berlin,*

*Arnimallee 6, D-14195 Berlin, Germany*

## Abstract

The curvature dependence of the physisorption properties of a water molecule inside and outside an armchair carbon nanotube (CNTs) is investigated by an incremental density–fitting local coupled cluster treatment with single and double excitations and perturbative triples (DF–LCCSD(T)) study. Our results show that a water molecule outside and inside $(n, n)$ CNTs ($n$=4, 5, 6, 7, 8, 10) is stabilized by electron correlation. The adsorption energy of water inside CNTs decreases quickly with the decrease of curvature (increase of radius) and the configuration with the oxygen pointing towards the CNT wall is the most stable one. However, when the water molecule is adsorbed outside the CNT, the adsorption energy varies only slightly with the curvature and the configuration with hydrogens pointing towards the CNT wall is the most stable one. We also use the DF–LCCSD(T) results to parametrize Lennard–Jones (LJ) force fields for the interaction of water both with the inner and outer sides of CNTs and with graphene representing the zero curvature limit. It is not possible to reproduce all DF–LCCSD(T) results for water inside and outside CNTs of different curvature by a single set of LJ parameters, but two sets have to be used instead. Each of the two resulting sets can reproduce three out of four minima of the effective potential curves reasonably well. These LJ models are then used to calculate the water adsorption energies of larger CNTs, approaching the graphene limit, thus bridging the gap between CNTs of increasing radius and flat graphene sheets.

## I. INTRODUCTION

In recent years, the study of water confined inside low–diameter carbon nanotubes (CNTs) has attracted a lot of attention because of many exotic properties that differ from those of the bulk phases [1–6]. Being confined in tubes with diameters not much larger than the size of the water molecules themselves, the topology of their hydrogen–bonding networks is dominated by unique structures such as water wires, different helix–like or prism–like ice nanotubes, both single– or multi–walled [7–9]. Consequently, there is also a variety of different phase transitions of water inside small CNTs not seen in bulk water, and in some cases it was predicted that ice nanotubes can even exist at room temperature [10, 11]. Moreover, spontaneous electric polarization was found to occur in some ice nanotubes confined inside CNTs [12–14]. Also the transport of water is strongly effected by the confinement in nanotubes. In particular, the greatly enhanced flow–rates are assigned to the smoothness of the CNT interior walls [15]. It is expected that these properties may give rise to applications of CNTs for, e.g., biomedical devices and efficient molecular separation [16, 17].

As long as microscopic experiments concerning the structure and dynamics of water confined in small CNTs are still very scarce, most of the work in the fields mentioned above is based on molecular simulations. Because of the large number of particles typically involved in molecular dynamics (MD) simulations of water in CNTs, practically all previous work was based on empirical force fields. In particular, Lennard–Jones (LJ) potentials are widely used to model the non–bonded carbon–water interactions and are available in most of the molecular dynamics software packages, providing an efficient way to simulate systems even with millions of atoms. However, there are large discrepancies in the values of the empirical LJ parameters used in previous studies of structure and dynamics of water confined in CNTs, see e.g. Tab. I in Ref. [9]. But already in one of the first simulation studies of water conduction in CNTs, it has been noticed that small changes in modelling the nanotube–water interaction can induce large differences in the water occupancy [18] and water filling kinetics and thermodynamics [19–22]. Also structure and dynamics of ice nanotubes confined inside CNTs were found to depend sensitively on the parameters of LJ potentials [13, 23]. Hence, it is a major challenge to obtain quantitatively correct values for those parameters. With the recent advances in computational resources, paralleled by progress in the developments of methods and algorithms, high–level quantum chemical methods have become available,

even for rather complex systems, such as the ones of interest here. Recently, the interaction of water with graphene has become a benchmark system for high–level quantum chemistry methods [24–28]. In fact, incremental CCSD(T) results for water adsorbed on graphene [29] are used to reparametrize LJ interaction models for MD simulations [23] of water confined inside CNTs. There an overall water–carbon interaction strength has been found, which is significantly stronger than in most previous simulations [11, 12, 18, 30–39]. Moreover, the results for the water–carbon interaction showed a rather strong anisotropy with respect to the water orientation, which was not considered in most of the previous work either, for an exception see Ref. [40].

The present work aims at accounting for the effect of the curvature of CNT walls on the interaction with water which has an important impact, e.g., on the transport properties [15, 41]. However, to the best of our knowledge, until recently there have been no high level *ab initio* results for the interaction of water with CNT systems but only density functional theory (DFT) results [40, 42]. Hence, we lately started to investigate these systems at a highly accurate quantum–chemistry level, namely an incremental density-fitting local coupled cluster treatment with single and double excitations and perturbative triples (DF–LCCSD(T)) [43], investigating the curvature dependent adsorption properties of a water molecule inside and outside $(n, n)$ CNT ($n$=4, 5, 6, 7, 8, 10) fragments. In order to save computational effort and to be able to treat even larger systems, the focus of this work is on a comparison of the computationally very demanding DF–LCCSD(T) method with different, less expensive methods: a) the computationally cheaper dispersion corrected DFT variants which are, however, not systematically improvable as the CCSD(T) method, and b) even cheaper LJ force fields for classical molecular dynamics simulations for larger CNTs, thus bridging the gap between CNTs of increasing radius and flat graphene sheets.

## II.  MODEL AND COMPUTATIONAL DETAILS

In order to explore the adsorption interaction between CNTs and water, the system is modelled by a single water molecule inside or outside $(n, n)$ CNT fragments ($n$= 4, 5, 6, 7, 8, 10), where the ends are saturated by $4n$ hydrogen atoms. The length of the CNT fragment (defined as distance between the two outer carbon rings perpendicular to the tube axis) in our simulation is 7.37 Å in all cases, which results in $14n$ carbon atoms for our $(n, n)$

3

CNT fragments. Based on the most stable configuration of water on a graphene surface [29], throughout this work we keep the water molecule to be located above the center site of a carbon ring and the two hydrogen atoms of the water molecule pointing towards C–C bonds along the axial direction of CNTs. In each case, two configurations are investigated, as displayed in Fig. 1. One of them is termed ∧–configuration, in which the two hydrogen atoms are closer to the wall of CNT than the oxygen atom. The other configuration is termed ∨–configuration, in which the oxygen atom is closer to the wall of CNT. Due to the high computational costs of the quantum chemistry methods discussed below, scans of water orientation angles are beyond our computational means. For the water molecule, the O–H bond lengths are set to be 0.958 Å and the H–O–H angle is set to be 104.45°. For armchair CNTs, the C–C distances are set to the experimental value of 1.421 Å. The dangling bonds of CNTs are saturated with hydrogen atoms with C–H distances set to 1.084 Å.

Highly accurate quantum–chemical CCSD(T) results using MOLPRO software [44] are obtained using the method of increments [45]. In order to reduce the computational effort with only a negligible effect on the accuracy for large systems, the DF–LCCSD(T) method are used [46]. The basis sets of the polarized correlation-consistent valence-double-$\zeta$ basis (cc–pVDZ) for C and H of CNTs and the aug–cc–pVTZ basis [47] for the O and H atom of water molecule are used for Hartree–Fock (HF) calculations and the corresponding basis for density–fitting for the local correlation treatments. A basis set test performed for water on graphene [29] shows that the used basis set is sufficiently accurate for the adsorption energy.

For comparison we also employ dispersion corrected density functional methods which are less time–consuming than CCSD(T) calculation. The PBE–D2/D3 calculations [48–50] are performed by using MOLPRO software [44] for the finite fragments and with projector augmented wave pseudopotentials as implemented in the Vienna ab–initio simulation package (VASP) [51, 52] for a periodic set–up. In the projector augmented wave method, the plane–wave kinetic energy cutoff is set to 400 eV. The Brillouin–zone integration is sampled with a single $k$–point. The CNT systems are modelled by using a (1×1×5) supercell to insure that the distance between a water molecule and its periodic image is more than 12 Å to avoid notable interaction between them. A comparison of the finite fragment PBE–D3 calculations (with the finite basis set (MOLPRO)) with the periodic modelling (with the plane-wave basis (VASP)) of the water inside and outside the CNT yields very good agreement, providing that the cluster model of the CNTs is sufficiently larger. The shape of the

4

potential energy curves and the positions of the minima agree very well, only the depth of all minima is deeper by about 20 meV in the plane–wave basis treatment.

Both for larger CNTs or for an increasing number of water molecules, even the computational effort of DFT calculations will be exceedingly high, at least for long–time molecular dynamics simulations. As an alternative, we aim here at obtaining reliable force field parameters by fitting effective water–CNT and water–graphene potentials to DF–LCCSD(T) results. To this end, we use the approximation of pairwise additive LJ potential energy functions which are often used to model non–bonded interactions:

$$V(r_{ij}) = 4 \sum_{\substack{i \in H_2O \\ j \in CNT}} \epsilon_{ij} \left[ \left( \frac{\sigma_{ij}}{r_{ij}} \right)^{12} - \left( \frac{\sigma_{ij}}{r_{ij}} \right)^{6} \right], \tag{1}$$

which sums the interactions between H and O atoms ($i$) of the water model and C atoms ($j$) in the CNT (or graphene) model. Here $\epsilon_{ij}$ represents the respective attractive well depth and $\sigma_{ij}$ is the root of the pair potential, i.e. the point where attractive and repulsive part of the LJ potential cancel. Note that our LJ potentials are also used to implicitly model the CNT polarization by the water dipole moment; hence no partial charges are involved throughout the present work. As will be shown in detail below, the $\sigma$ parameters are very close to the sums at the respective van der Waals radii and none or only minor adjustments are necessary. In contrast, optimal values for the $\epsilon$ parameters are under debate in the literature [23]. Hence, we scanned the range of those parameters manually, striving for good agreement with the current CCSD(T) results. An automated fitting procedure yielding also statistics of the deviations such as, e.g. in Ref. [53], is not employed here because of the very small number of parameters (see Sec. III for details) and because of the relatively small data sets obtained from the quantum chemical calculations.


## III.   RESULTS AND DISCUSSION

To quantify the curvature effect, we calculate the adsorption energies of a water molecule inside and outside of armchair $(n, n)$ CNT fragments ($n$=4, 5, 6, 7, 8, 10). The position of the center of mass of the water molecule which respect to the longitudinal axis of the $(n, n)$ CNT is labelled with $x$. Negative values correspond to the ∧–configuration outside CNTs and ∨–configuration inside CNTs, while positive values for ∧–configuration inside CNTs and ∨–configuration outside CNTs, as shown in Fig. 1(a) from left to right.

Our DF-LCCSD(T) results are compiled in Tab. I. It is immediately seen that the adsorption energies of water inside CNTs are much stronger than those for water outside CNTs, because in the former case the attractive dispersive forces from the all sides of the nanotube contribute to the interaction energy add up [43]. In the later case, however, the water molecule essentially only interacts with one side of the CNT. When the water molecule adsorbed outside $(n, n)$ CNTs (see Fig 2(a) and (d) for $n$=5, Fig. 2(e) and (h) for $n$=6, Tab. I for all cases), the DF–LCCSD(T) adsorption energy of the $\wedge$–configuration is always lower than the one of the $\vee$–configuration. For the smallest armchair CNT (4,4) investigated, a DF–LCCSD(T) adsorption energy of $\vee$–configuration of water outside is -99 meV, while -136 meV for the $\wedge$–configuration (not shown in Fig. 2). The adsorption energy curves for a water molecule outside $(6, 6)$ CNT are very similar to those for water outside $(4, 4)$ and $(5, 5)$ CNTs and show nearly no curvature effects. Note that the adsorption energies of water outside $(n, n)$ CNTs , see Tab. I also for larger CNTs, are close to the results of a water molecule adsorbed on a graphene surface, including the energy differences between $\wedge$– and $\vee$–configurations which are -123 and -108 meV, respectively [29].

Next, we will discuss three typical cases of a water molecule inside CNTs. First, water inside $(4, 4)$ CNT shows purely repulsive interactions indicating that water molecules do not permeate spontaneously, since a $(4, 4)$ CNT has a too small tube radius, $R$=2.65 Å, to accommodate water molecules inside. Second, for $n$=5 the energy curves have only one minimum for water inside CNT corresponding to a $\vee$–configuration, as shown in Fig. 2(b). Therefore, this is the narrowest armchair CNT to adsorb water molecules inside. The third typical case is $n$=6. As shown in Fig. 2(f) and 2(g), two minimum energy structures are predicted inside a $(6,6)$ CNT by our DF–LCCSD(T) calculations. Also for larger diameter CNTs we find two minima at the DF–LCCSD(T) level of theory, in all cases with the $\vee$– configuration slightly more stable than the $\wedge$–configuration. An important result is that the investigated CNTs display an obvious curvature effect on water adsorbed inside them as listed in Tab. I. The adsorption energy decreases quickly with decreasing wall curvature (increasing CNT radius $R$) from $n$=5 to 10 approaching the graphene limit, $1/R \rightarrow 0$ (see open symbols in Fig. 3). While the adsorption energy of water inside a $(5,5)$ CNT is nearly four times as large as the outside case, for the $(10,10)$ CNT the energies of water inside and outside become close to each other. A change in the order of the stabilities of $\vee$– and $\wedge$– configuration has to occur for large diameter CNTs, because for the adsorption on graphene

6

the ∧–configuration is more stable.

As also shown in Tab. I, the stable configurations predicted by using MP2 are the same as the DF–LCCSD(T) for a water molecule adsorbed inside CNTs. The MP2 calculations also reproduce the same tendencies of the adsorption curves but with a little higher energies than the DF–LCCSD(T) results. However, the VASP results for PBE–D2 and PBE–D3 are different for inside and outside cases. For the outside cases, PBE–D3 method gives a better description of dispersion correlation than PBE–D2. For the inside case, where the DF–LCCSD(T) calculations report two pronounced minima for $n \geq 6$ and the ∨–configuration as the more stable one, both PBE–D2 and PBE–D3 predict only the ∧–configuration as the stable one.

Another goal of the present work is to use the DF–LCCSD(T) results to parametrize force fields for the interaction of a single water molecule with graphene as well with CNTs (inside and outside). First, we consider our previous LJ model for the CO and CH interaction between oxygen and hydrogen atoms in the water molecule and all of the carbon atoms, obtained by fitting to CCSD(T) calculations for the water–graphene interaction only [23, 29], shown in the first row (# 1) of Tab. II. As can be seen from the blue curves in Fig. 4, this model cannot reproduce our DF–LCCSD(T) results for the CNTs. In general, the interaction strength is weaker than predicted by DF–LCCSD(T), especially for water outside the CNTs. Upon considerably increasing the attractive well depth $\epsilon_{CH}$ between carbon and hydrogen and slightly readjusting the two $\sigma$ parameters, (row # 2 in Tab. II and red curves in Fig. 4), the potential energy curves for water adsorbed outside CNTs are reproduced satisfactorily. However, the curves for water inside CNTs are considerably more attractive than the DF–CCSD(T) results, especially when hydrogen is pointing towards the CNT wall (∧–configuration). Hence, the energetic ordering of ∨– and ∧–configurations is exchanged, as was also found for parameter set # 1. Our Fig. 4 shows also results for water–graphene systems, where (A), (B) and (C) are labelling configurations where the water molecule is on top of an atom, on a bond site or a ring center site, respectively. For case (A), set # 2 describes the adsorption energy better than set # 1; conversely, for case (B) and (C), parameter set # 1 is superior.

To solve the problem of the energetic ordering of ∨– and ∧–configurations for water inside CNTs, we suggest a modified LJ model for the water–carbon interaction where the oxygen interaction site is replaced by two neutral dummy particles (labelled as X in Tab. II)

representing the polarizability of the lone pair electrons of water, using the same positions as in the TIP5P force field [54]. The model with the lone pair dummies stabilizes the ∨– configuration inside the CNTs due to a better description of the polarizability of the oxygen atom, since the main contribution to the binding is the induced dipole–dipole interaction of the water molecule with the $\pi$–electron density of the CNTs [43], and therefore the description of the polarizability of the oxygen atom was improved in the LJ model. It can be seen in Fig. 5 that the new model describes the potential energy curves much better, especially for the ∨–configuration of water inside $(n, n)$ CNTs. Two sets of parameters obtained by manually scanning the $\epsilon$ and $\sigma$ parameters for the CH and CX interaction are listed as # 3 and # 4 in Tab. II and shown as blue and red curves, respectively, in Fig. 5. These two sets of LJ parameters have different advantages and disadvantages in describing the potential energy in the different cases. Parameter set # 3 describes the potential energy inside CNTs everywhere very well and the ∨–configuration (but not the ∧–configuration) for water outside CNTs. In contrast, parameter set # 4 describes the potential energy outside CNTs everywhere very well and also the ∨–configuration (but not the ∧–configuration) for water inside CNTs. Note that, within the restrictions of the simple LJ model, it was not possible to find one set of parameters describing the four minima for each of the CNTs equally well. Hence, in practical MD simulations, one of these two sets of parameters can be chosen, depending on the different confinement conditions of water molecules. In describing the water–graphene adsorption energy, parameter set # 4 is better than parameter # 3 for sites (A) and vice versa for sites (B) and (C).

The resulting LJ models can be used to predict also the interaction of water with CNTs of much larger radius which are currently out of reach for high level quantum chemistry. Calculated data for parameter sets # 3 and # 4 for armchair CNTs $(n, n)$ with $n$=12, 14, 16, 18, 22, 30, 34, 38, 42 are also included as full symbols in Fig. 3. Parameter set # 3 reasonably reproduces the magnitude of the water–graphene interaction for the inside adsorption minima, but the order of the ∧– and ∨–configuration is wrong in the limit, $1/R \to 0$. Using parameter set # 4 for the extrapolation to the graphene limit, the ∧–configuration is stabilized against the ∨–configuration, but too strong, so the magnitude of the adsorption energy is overestimated. However, set # 4 can reproduce the transition from the most stable ∨–configuration inside small CNTs to the most stable ∧–configuration for larger CNTs and graphene leading to a crossing of the corresponding curves. Parameter set

# 4 predicts a radius of about 10 Å which corresponds to a (14,14) CNT for the crossing. For larger radii the ∧–configuration is also the most stable one inside the CNTs.


## IV. SUMMARY AND CONCLUSIONS

The physisorption properties of a water molecule interacting with $(n, n)$ CNTs with $n$=4, 5, 6, 7, 8, 10 are investigated by performing DF–LCCSD(T) calculations. Our main result is that the physisorption properties of water molecule outside and inside carbon nanotube display a different curvature dependence of the adsorption energies. For the outside case, there is only little effect of the curvature, however, for the inside case, the magnitude of the adsorption energy is decreasing with decreasing CNT curvature of CNT wall, tending toward the graphene results. By fitting LJ parameters to our high quality DF–LCCSD(T) quantum chemistry results, we were able to derive simple but reliable models for carbon sheets of different curvature. In particular, by adding dummy particles mimicking the polarizability of the oxygen atom we improved the quality of atom–centered LJ models. This model reproduces all DF–LCCSD(T) results for water inside and outside CNTs of different curvature by two sets of LJ parameters. Each of them can reproduces three out of four minima of the effective potential curves reasonably well. These LJ models are used to calculate the water adsorption energies of larger CNTs, approaching the graphene limit, thus bridging the gap between CNTs of increasing radius and flat graphene sheets. Finally, we mention that, in agreement with our previous findings for water interacting with graphene [23, 29], the overall carbon–water interaction strength obtained from fitting to the current DF–LCCSD(T) results for water interaction with CNTs is considerably stronger than assumed in most of the previous classical MD simulations [9, 38], with the exception of the work presented in Refs. [40] and [55]. Hence, the present work suggests that the CNTs may be less hydrophobic than commonly anticipated.

---

[1] J. Martí and M. C. Gordillo, *Phys. Rev. B*, 2001, **63**, 165430.

[2] J. Martí and M. C. Gordillo, *J. Chem. Phys.*, 2001, **114**, 10486.

[3] J. Martí and M. C. Gordillo, *Phys. Rev. E*, 2001, **64**, 021504.

[4] L. Wu, F. Wu, J. Kou, H. Lu and Y. Liu, *Phys. Rev. E*, 2011, **83**, 061913.

[5] Z. He, J. Zhou, X. Lu and B. Corry, *J. Phys. Chem. C*, 2013, **117**, 11412.

[6] W. Zhao, L. Wang, J. Bai, J. S. Francisco and X. C. Zeng, *J. Am. Chem. Soc.*, 2014, **136**, 10661.

[7] M. C. Gordillo and J. Martí, *Chem. Phys. Lett.*, 2000, **329**, 341.

[8] D. Tasis, N. Tagmatarchis, A. Bianco and M. Prato, *Chem. Rev.*, 2006, **106**, 1105–1136.

[9] A. Alexiadis and S. Kassinos, *Chem. Rev.*, 2008, **108**, 5014.

[10] H. Kyakuno, K. Matsuda, H. Yahiro, Y. Inami, T. Fukuoka, Y. Miyata, K. Yanagi, Y. Maniwa, H. Kataura, T. Saito, M. Yumura and S. Iijima, *J. Chem. Phys.*, 2011, **134**, 244501.

[11] D. Takaiwa, I. Hatano, K. Koga and H. Tanaka, *Proc. Natl. Acad. Sci.*, 2008, **105**, 39–43.

[12] C. Luo, W. Fa, J. Zhou, J. Dong and X. C. Zeng, *Nano Lett.*, 2008, **8**, 2607.

[13] S. Li and B. Schmidt, *Phys. Chem. Chem. Phys.*, 2015, **17**, 7303.

[14] Y. Nakamura and T. Ohno, *Phys. Chem. Chem. Phys.*, 2011, **13**, 1064–1069.

[15] K. Falk, F. Sedlmeier, L. Joly, R. R. Netz and L. Bocquet, *Nano Lett.*, 2010, **10**, 4067–4073.

[16] T. Ohba, *Angew. Chem. Int. Ed.*, 2014, **53**, 8032.

[17] J. Kou, H. Lu, F. Wu, J. Fan and J. Yao, *Nano Lett.*, 2014, **9**, 4931.

[18] G. Hummer, J. C. Rasaiah and J. P. Noworyta, *Nature*, 2001, **414**, 188.

[19] A. Waghe, J. C. Rasaiah and G. Hummer, *J. Chem. Phys.*, 2002, **117**, 10789.

[20] S. Vaitheeswaran, J. C. Rasaiah and G. Hummer, *J. Chem. Phys.*, 2004, **121**, 7955–7965.

[21] S. Sriraman, I. G. Kevrekidis and G. Hummer, *Phys. Rev. Lett.*, 2005, **95**, 130603.

[22] A. Waghe, J. C. Rasaiah and G. Hummer, *J. Chem. Phys.*, 2012, **137**, 044709.

[23] G. Pérez-Hernández and B. Schmidt, *Phys. Chem. Chem. Phys.*, 2013, **15**, 4995.

[24] E. M. Cabaleiro-Lago, J. A. Carrazana-García and J. Rodríguez-Otero, *J. Chem. Phys.*, 2009, **130**, 234307.

[25] G. R. Jenness and K. D. Jordan, *J. Phys. Chem. C*, 2009, **113**, 10242.

[26] G. R. Jenness, O. Karalti and K. D. Jordan, *Phys. Chem. Chem. Phys.*, 2010, **12**, 6375.

[27] M. Rubeš, P. Nachtigall, J. Vondrášek and O. Bludský, *J. Phys. Chem. C*, 2009, **113**, 8412.

[28] M. Rubeš, J. Kysilka, P. Nachtigall and O. Bludský, *Phys. Chem. Chem. Phys.*, 2010, **12**, 6438.

[29] E. Voloshina, D. Usvyat, M. Schütz, Y. Dedkov and B. Paulus, *Phys. Chem. Chem. Phys.*, 2011, **13**, 12041–12047.

[30] K. Koga, R. D. Parra, H. Tanaka and X. C. Zeng, *J. Chem. Phys.*, 2000, **113**, 5037.

[31] K. Koga, G. Gao, H. Tanaka and X. C. Zeng, *Nature*, 2001, **412**, 802.

[32] A. Berezhkovskii and G. Hummer, *Phys. Rev. Lett.*, 2002, **89**, 064503.

[33] W. H. Noon, K. D. Ausman, R. E. Smalley and J. Ma, *Chem. Phys. Lett.*, 2002, **355**, 445.

[34] R. J. Mashl, S. Joseph, N. R. Aluru and E. Jakobsson, *Nano Lett.*, 2003, **3**, 589–592.

[35] A. I. Kolesnikov, J.-M. Zanotti, C.-K. Loong, P. Thiyagarajan, A. P. Moravsky, R. O. Loutfy and C. J. Burnham, *Phys. Rev. Lett.*, 2004, **93**, 035503.

[36] J. Wang, Y. Zhu, J. Zhou and X.-H. Lu, *Phys. Chem. Chem. Phys.*, 2004, **6**, 829–835.

[37] J. Bai, J. Wang and X. C. Zeng, *Proc. Natl. Acad. Sci.*, 2006, **103**, 19664.

[38] A. Alexiadis and S. Kassinos, *Chem. Eng. Sci.*, 2008, **63**, 2047.

[39] J. Köfinger, G. Hummer and C. Dellago, *Proc. Natl. Acad. Sci.*, 2008, **105**, 13218.

[40] M. Kaukonen, A. Gulans, P. Havu and E. Kauppinen, *J. Comput. Chem.*, 2012, **33**, 652.

[41] Y. Liu and Q. Wang, *Phys. Rev. B*, 2005, **72**, 085420.

[42] M. Rajarajeswari, K. Iyakutti and Y. Kawazoe, *Phys. Status. Solidi. B*, 2011, **248**, 1431.

[43] S. Lei and B. Paulus, *Water molecule inside and outside armchair carbon nanotube: a method of incremental study, to be published*.

[44] H.-J. Werner, P. J. Knowles, G. Knizia, F. R. Manby, M. Schütz *et al.*, *MOLPRO, version 2012.1, a package of ab initio programs*, 2012, see http://www.molpro.net.

[45] H. Stoll, *J. Chem. Phys.*, 1992, **97**, 8449–8454.

[46] H.-J. Werner and M. Schütz, *J. Chem. Phys.*, 2011, **135**, 144116.

[47] T. H. Dunning Jr, *J. Chem. Phys.*, 1989, **90**, 1007.

[48] J. P. Perdew, K. Burke and M. Ernzerhof, *Phys. Rev. Lett.*, 1996, **77**, 3865.

[49] S. Grimme, *J. Comp. Chem.*, 2006, **27**, 1787.

[50] S. Grimme, J. Antony, S. Ehrlich and H. Krieg, *J. Chem. Phys.*, 2010, **132**, 154104.

[51] G. Kresse and J. Furthmüller, *Comp. Mater. Sci.*, 1996, **6**, 15.

[52] G. Kresse and J. Furthmüller, *Phys. Rev. B*, 1996, **54**, 11169.

[53] V. W. Ruangpornvisuti, M. M. Probst and B. M. Rode, *Zeitschrift für Naturforschung A*, 1987, **42**, 871–874.

[54] M. W. Mahoney and W. L. Jorgensen, *J. Chem. Phys.*, 2000, **112**, 8910.

[55] M. Melillo, F. Zhu, M. A. Snyder and J. Mittal, *J. Phys. Chem. Lett.*, 2011, **2**, 2978.

TABLE I. Adsorption energies (in meV) of a water molecule outside and inside $(n, n)$ CNT with $n$=5, 6, 7, 8, 10 for ∧–configurations and ∨–configurations for various quantum chemistry methods. The values in parentheses are minimum energy positions (in Å) along $x$ axis as shown in Fig. 1(a). The PBE–D2/D3 are from periodic calculations using VASP [48–52].

| Configurations | | Methods | (5,5) | (6,6) | (7,7) | (8,8) | (10,10) |
|---|---|---|---|---|---|---|---|
| Outside | ∧ | DF–LCCSD(T) | -126(-6.6) | -128(-7.3) | -128(-7.9) | -127(-8.7) | -124(-10.1) |
| | | MP2 | -117(-6.6) | -117(-7.3) | -118(-8.0) | -115(-8.7) | -110(-10.1) |
| | | PBE–D2 | -130(-6.4) | -131(-7.1) | -133(-7.8) | -134(-8.5) | -136(-9.9) |
| | | PBE–D3 | -124(-6.6) | -124(-7.3) | -127(-8.0) | -128(-8.7) | -131(-10.1) |
| | ∨ | DF–LCCSD(T) | -103(6.1) | -103(6.8) | -104(7.5) | -101(8.2) | -96(9.6) |
| | | MP2 | -86(6.1) | -87(6.9) | -88(7.6) | -85(8.3) | -79(9.6) |
| | | PBE–D2 | -82(6.3) | -81(7.0) | -83(7.7) | -82(8.4) | -84(9.8) |
| | | PBE–D3 | -88(6.4) | -89(7.1) | -91(7.8) | -91(8.5) | -93(9.9) |
| Inside | ∧ | DF–LCCSD(T) | -404(0.0) | -262(0.5) | -199(1.4) | -171(2.1) | -145(3.5) |
| | | MP2 | | -235(0.5) | -176(1.3) | -150(2.1) | -134(3.5) |
| | | PBE–D2 | -357(0.0) | -282(0.8) | -237(1.5) | -213(2.3) | -190(3.7) |
| | | PBE–D3 | | -312(0.5) | -249(1.3) | -219(2.1) | -192(3.5) |
| | ∨ | DF–LCCSD(T) | | -279(-0.9) | -214(-1.7) | -182(-2.5) | -148(-3.9) |
| | | MP2 | -364(-0.1) | -257(-0.9) | -197(-1.7) | -166(-2.4) | -143(-3.9) |
| | | PBE–D2 | | | -167(-1.5) | -144(-2.3) | -121(-3.8) |
| | | PBE–D3 | -378(-0.1) | | -202(-1.5) | -169(-2.3) | -142(-3.7) |

| # | $\epsilon_{CO}$ | $\epsilon_{CH}$ | $\epsilon_{CX}$ | $\sigma_{CO}$ | $\sigma_{CH}$ | $\sigma_{CX}$ |
|---|---|---|---|---|---|---|
| 1 | 5.182 | 2.591 | | 3.16 | 2.73 | |
| 2 | 5.182 | 4.457 | | 3.00 | 2.80 | |
| 3 | | 3.835 | 3.6274 | | 2.85 | 2.60 |
| 4 | | 6.633 | 2.178 | | 2.75 | 2.65 |

TABLE II. LJ potential parameters for water–carbon interaction, see Eq. (1), where $\epsilon$ represents the attractive well depth (in meV) and $\sigma$ is the distance at which the pair potential is zero (in Å). Subscripts C, O, H and X are for carbon, oxygen, hydrogen and dummy particles of water respectively (no partial charges involved). Row # 1: previous fit to CCSD(T) calculations of graphene–water from Ref. [23]. # 2–4: fit to the present DF–LCCSD(T) calculations of $(n, n)$ CNT–water for $n = 5, 6, 7, 8, 10$.
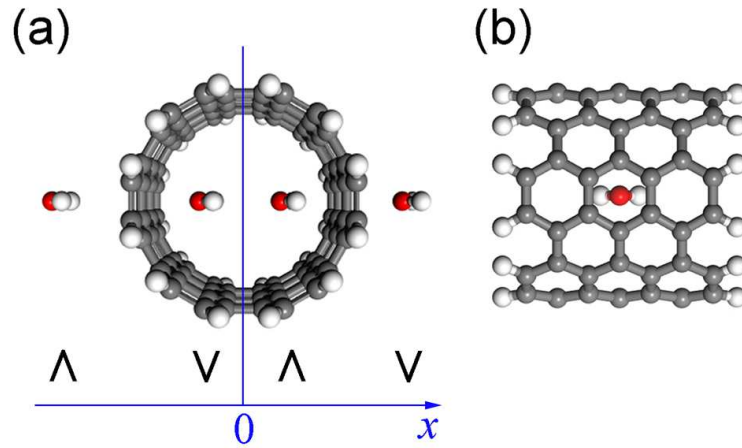
FIG. 1. Adsorption structures of a water molecule inside and outside a (6,6) CNT fragment. (a) top view for ∨–configuration outside, ∧–configuration inside, ∨–configuration inside and ∧–configuration outside CNT (from left to right) and (b) side view.
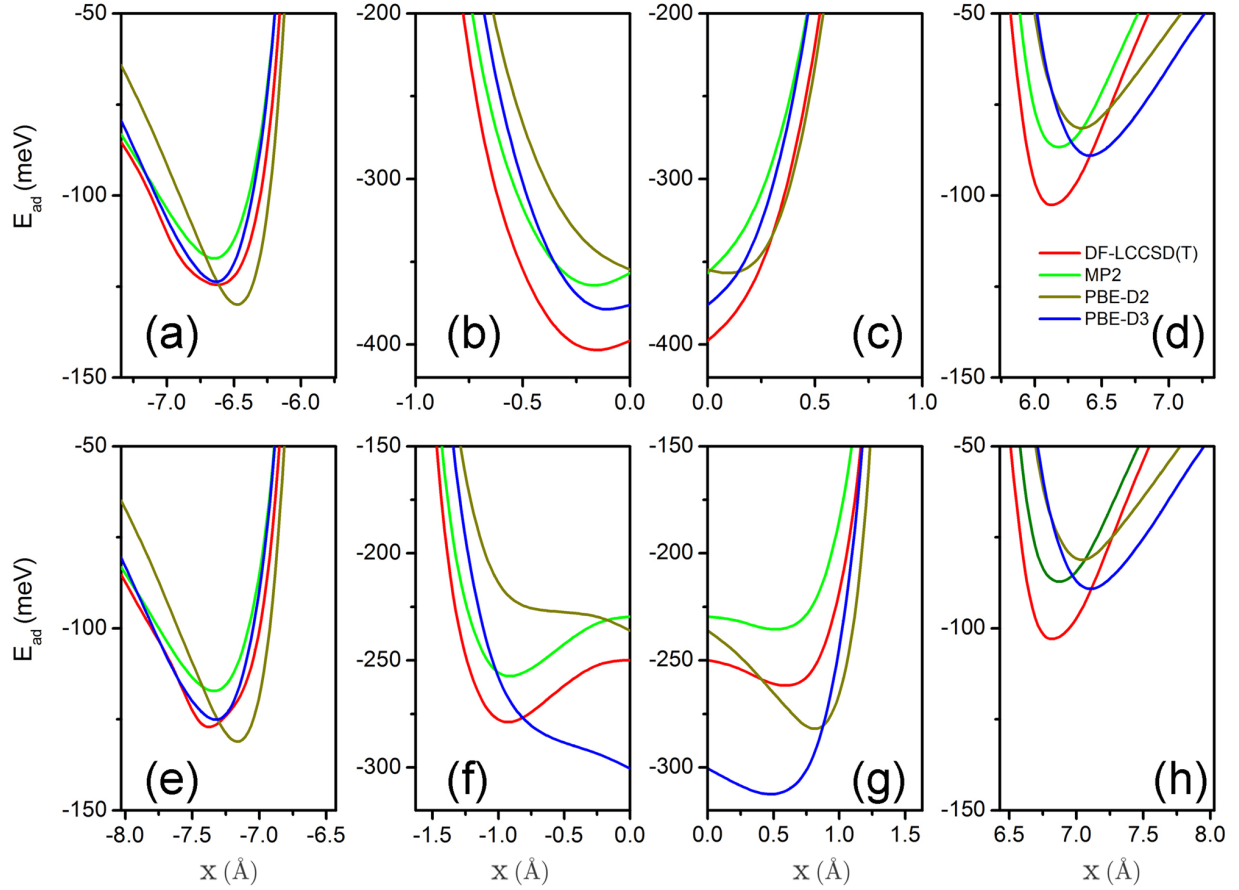
FIG. 2. Adsorption energies of water inside and outside CNTs for different methods as a function of the position $x$. (a) $\wedge$ outside, (b) $\vee$ inside, (c) $\wedge$ inside and (d) $\vee$ outside (5,5) CNT. (e)~(h) same for (6,6) CNT. The PBE–D2/D3 are from periodic calculations using VASP [48–52].
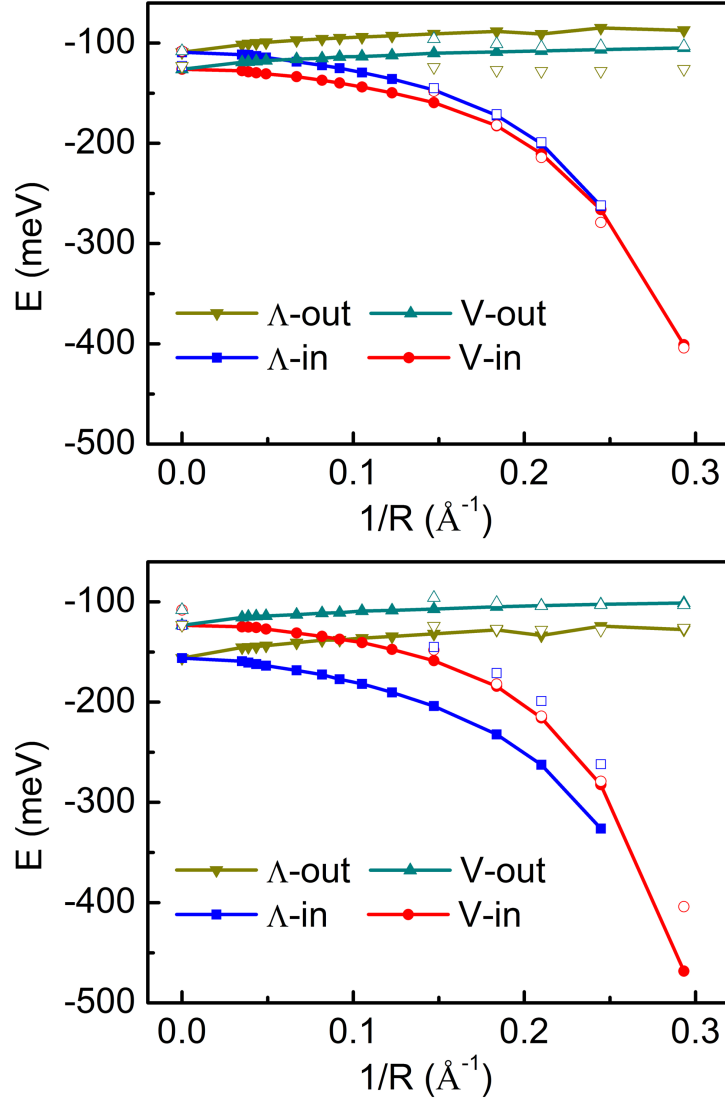
FIG. 3. Curvature dependence of the four minima of the effective potential energy curves of water inside and outside CNTs. Open symbols: DF–LCCSD(T) results for CNTs, (see also Tab. I) and CCSD(T) results for graphene, $1/R \rightarrow 0$, from Ref. [29]. Full symbols with curves: LJ model with parameter set # 3 (upper part) and # 4 (lower part), also Tab. II
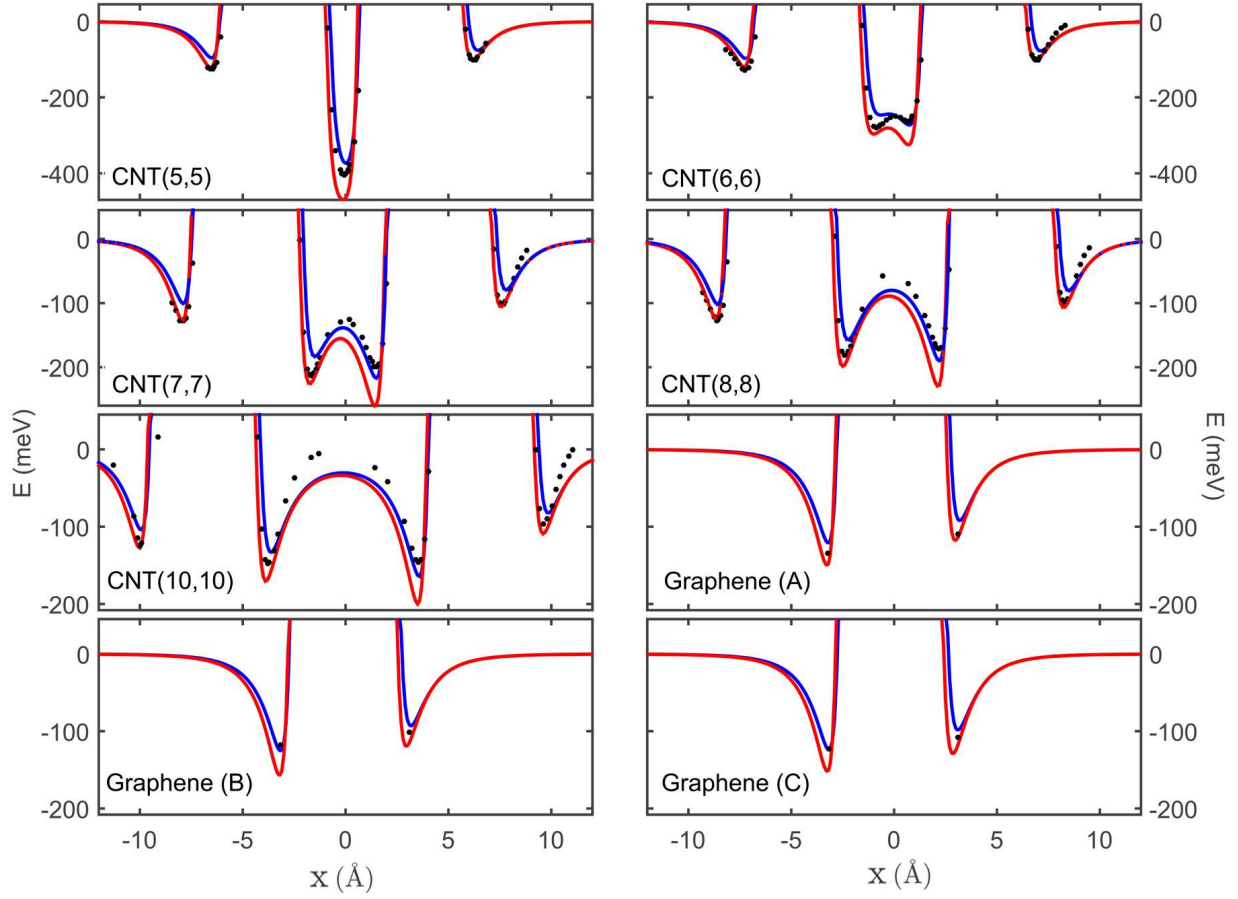
FIG. 4. Scan of the potential energy of a water molecule traversing various CNTs and graphene. Force fields # 1 from previous work [23] (blue) and # 2 (red) with interaction sites for water O and H, for parameters see Tab. II. Black points represent DF–LCCSD(T) results of the present work for CNTs and CCSD(T) results of previous work [29] for graphene.
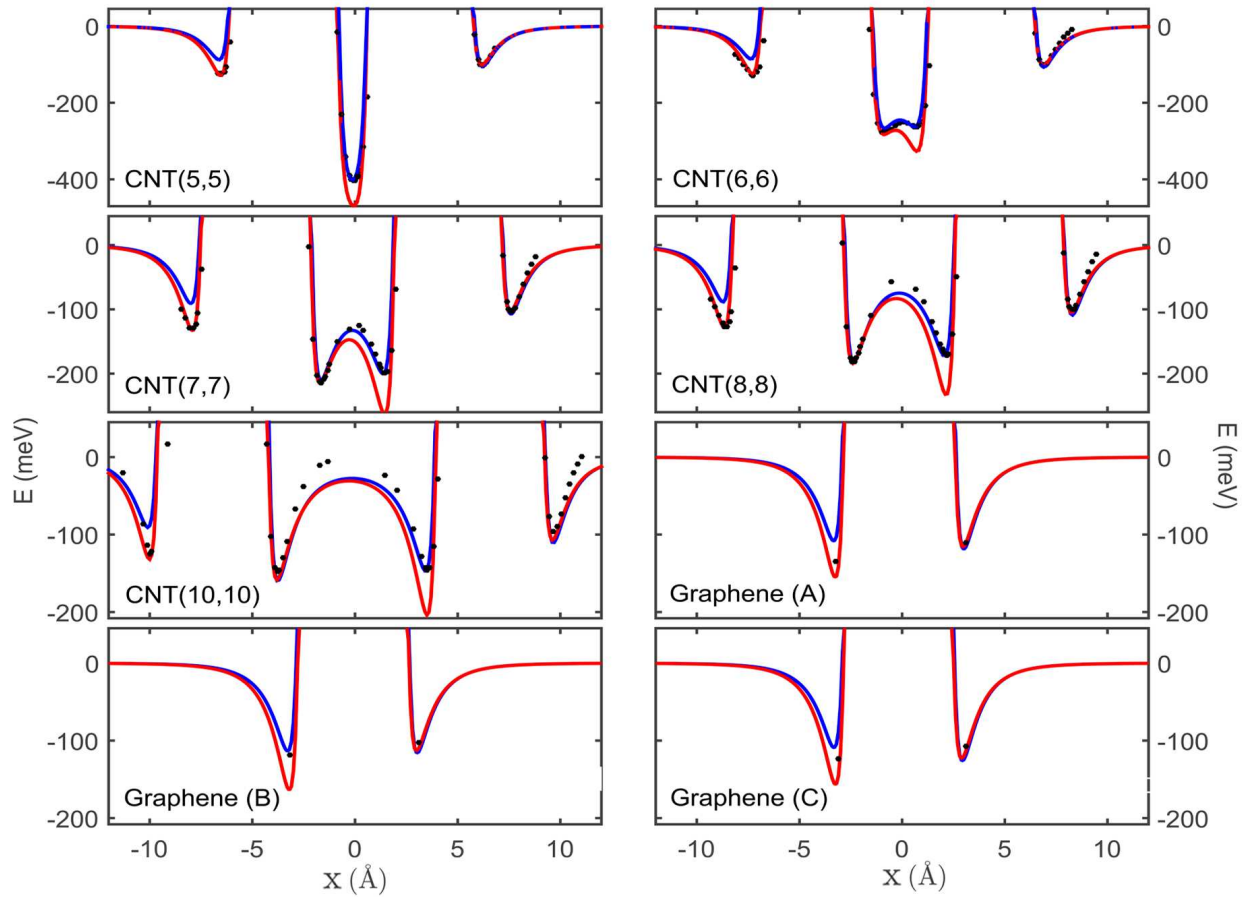
FIG. 5. Same as Fig. 4 but for a modified LJ model with additional dummy particles representing the lone pairs of the water molecule. Force fields # 3 (blue) and # 4 (red), for parameters see Tab. II.